# An indicator sensor criterion for in-situ characterisation of source vibrations

van der Seijs, Maarten; de Klerk, Dennis; Wernsen, M.W.F.

**Citation (APA)**
van der Seijs, M., de Klerk, D., & Wernsen, M. W. F. (2017). An indicator sensor criterion for in-situ characterisation of source vibrations. In E. Wee Sit, C. Walber, P. Walter, & S. Seidlitz (Eds.), *Sensors and Instrumentation, Proceedings of the 35th IMAC: A conference and Exposition on Structural Dynamics 2017* (Vol. 5, pp. 55-69). (Conference Proceedings of the Society for Experimental Mechanics Series ). Springer. https://doi.org/10.1007/978-3-319-54987-3_7

**Important note**
To cite this publication, please use the final published version (if applicable).
Please check the document version above.

# Chapter 7
# An Indicator Sensor Criterion for In-Situ Characterisation of Source Vibrations

**M.W.F. Wernsen, M.V. van der Seijs, and D. de Klerk**

**Abstract** Component-based Transfer Path Analysis allows us to analyse and predict vibration propagation between an active source and passive receiver structures. The forces that characterise the active source are determined using sensors placed on the connected passive substructure. These source characterisation forces, often called blocked or equivalent forces, are an inherent and unique property of the source, allowing to predict vibration levels in assemblies with different connected passive structures. In order to obtain a unique and accurate characterisation, accurate measurements are of key importance. The success of the characterisation is not only dependent on the hammer skill of the experimentalist, but also relates to sensor placement, overdetermination and matrix conditioning. In this paper the effects of each of these influences are studied using theoretical approaches, numerical studies and measurements on a benchmark structure designed for in-situ source characterisation. An assembly of two substructures is tested, representing an active substructure with a source and a passive substructure. In order to determine a criterion for the placement of indicator sensors, the effect of the various influences on the in-situ characterisation is compared. Using the results, a structured approach for the use of indicator sensors for in-situ blocked force TPA is proposed.

**Keywords** Transfer path analysis • Dynamic substructuring • Source characterisation • Blocked force • In-situ • Indicator sensors

## 7.1 Introduction

Knowledge of the vibrations of a system is essential in designing mechanically and acoustically sound products. With the current trend of modular design, in which different companies design specific parts for the final product, predicting the dynamic and acoustic qualities of the final product in an early design stage becomes more difficult. A useful tool to assess these qualities is Transfer Path Analysis (TPA). Using TPA, a vibrationally active source can be represented by a set of forces, relating to a certain dynamic load case. This characterisation can be used by engineers to calculate the dynamic response of the assembled system and track down the critical paths of vibration transmission.

There are many different flavours of TPA [1] and the ones most suited to solve source characterisation problems are from the category component-based TPA [2–4]. The useful property of component-based TPA methods is that the source can be characterised by forces that are inherent to the source structure only. Any assembly of this source structure with a passive structure can be simulated for, without the need to do a new operational measurement on the source. In practice this means that a company can characterise their active source structure on an in-house test bench and use this characterisation to predict sound and vibrations in the assembled product, or put more general: a characterisation of source A done in an assembly AB is also valid for use with any other passive side B.

The forces that characterise a source are often called *equivalent* or *blocked forces*, as they represent blocking forces that would be generated if the source structure was mounted to a rigid boundary. Yet a more practical method to obtain them is by measuring vibration responses in an assembly using acceleration sensors on the passive side. In a second step, Frequency Response Functions (FRFs) are obtained using for instance impact hammer measurements on the assembly. A matrix-inverse

---

M.W.F. Wernsen (✉) • D. de Klerk
Department of Precision and Microsystems Engineering, Delft University of Technology, Mekelweg 2, 2628CD, Delft, The Netherlands

VIBES.technology, Molengraaffsingel 14, 2629, Delft, JD, The Netherlands
e-mail: mwernsen@live.nl

M.V. van der Seijs
VIBES.technology, Molengraaffsingel 14, 2629, Delft, JD, The Netherlands

procedure is performed afterwards to determine the forces that exactly represent those vibrations. This approach is popularly known as *in-situ characterisation* [5], and is particularly effective for characterisation in the original assembly (hence the name 'in-situ').

Combining concepts of TPA with the knowledge of Dynamic Substructuring (DS) [6] has led to a component TPA approach in which the source is characterised using forces and moments in a virtual point (VP) [7]. The virtual point has the advantage that it allows for easy coupling between two substructures, taking into account rotational coupling (and thus moments in the coupling points) as well. Implementing DS and VP technology gives rise to a modern approach for TPA [1], in which substructures can easily be coupled, source characterisations can be exchanged and in which numerical and experimental models can be merged to create hybrid simulations.

To ensure that a characterisation truly represents the source excitation and is property of solely the active substructure, the experimental procedures should meet certain requirements. Apart from the impact hammer skills of the experimentalist (which should be outstanding), the results of the characterisation highly depend on choices regarding sensor placement, overdetermination and matrix conditioning.

Some theoretical methods have been proposed that give an indication of the ideal location to place sensors for force identification. Examples are methods based on conditioning such as the composite conditioning number [8], or methods based on energy and system modes [9]. However, almost all of these methods require an accurate numerical model of the structure. Small errors of the model will have a large influence on the results and the results are specific for a certain structure and load case. As a numerical model often does not suffice to truly represent the experimental structure for moderate to high frequencies (typically above 500 Hz), such methods will not provide a suitable solution. Hence, a structured approach is needed for the use of indicator sensors that does not require a numerical model. Instead, by answering rudimentary questions such as where to place the sensors with respect to the excitation, one should be able to choose a set of indicator sensor locations that will yield the best possible characterisation.

### 7.1.1 Paper Outline

In this paper the influence of sensor placement, overdetermination and matrix conditioning is investigated using experimental measurements on a benchmark structure, substantiated by insights from numerical models. Section 7.2 of the paper will present the theory behind TPA and the methods used to perform source characterisation. In Sect. 7.3 the problems are identified that influence the quality of a characterisation using experimental data. Section 7.4 introduces the experimental structure used for this paper and presents the results of the measurements on this structure, identifying the effects of varying sensor locations and overdetermination on the quality of the source characterisation.

## 7.2 Theory

### 7.2.1 Component-Based TPA

Figure 7.1 shows the presence of two forces: the unknown and unmeasurable source excitation, represented by $\mathbf{f}_1$, and the equivalent forces that are used to characterise the source, represented by $\mathbf{f}_2^{\text{eq}}$. Furthermore, two response locations are shown, namely the responses of interest at the structure B, $\mathbf{u}_3$, and the indicator sensor responses $\mathbf{u}_4$ used for the in-situ characterisation of source $\mathbf{f}_1$, also located on structure B.

The fundamental difference between component-based TPA and other types of TPA is that the forces $\mathbf{f}_2^{\text{eq}}$ obtained from the characterisation are a property of substructure A only, and thus not depending on structure B. A physical interpretation can therefore be that when the equivalent forces are applied in the opposite direction *with the source in operation*, no responses should be present onward from $\mathbf{u}_2$. If the source is now deactivated, the response $\mathbf{u}_3$ for the assembled system AB, due to application of $\mathbf{f}_2^{\text{eq}}$, should be equal to the original responses caused by the active source. Using the assembled FRF matrix $\mathbf{Y}^{\text{AB}}$, with elements $Y_{ij}^{\text{AB}}$ representing the response at degree of freedom (DoF) $i$ due to a unit force excitation at DoF $j$, this relation can be expressed as follows:

$$\mathbf{u}_3(\omega) = \mathbf{Y}_{32}^{\text{AB}}(\omega)\mathbf{f}_2^{\text{eq}}(\omega) \tag{7.1}$$

**Fig. 7.1** An overview of the nodes and DoFs in assembly AB
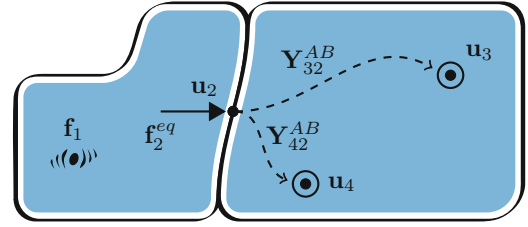


For the sake of notation all equations may be assumed to be in the frequency domain, unless otherwise stated, and $\omega$ is therefore emitted from the coming equations.

Expanding the assembled admittance using the substructures' admittances gives:

$$\mathbf{u}_3 = \mathbf{Y}_{32}^{AB}\mathbf{f}_2^{eq} = \left[\mathbf{Y}_{32}^{B}(\mathbf{Y}_{22}^{A} + \mathbf{Y}_{22}^{B})^{-1}\mathbf{Y}_{22}^{A}\right]\mathbf{f}_2^{eq} \tag{7.2}$$

As the response at $\mathbf{u}_3$ due to application of $\mathbf{f}_2^{eq}$ and $\mathbf{f}_1$ should be equal, the following relation for the forces can be deduced:

$$\mathbf{Y}_{32}^{B}(\mathbf{Y}_{22}^{A} + \mathbf{Y}_{22}^{B})^{-1}\mathbf{Y}_{22}^{A}\mathbf{f}_2^{eq} = \mathbf{Y}_{32}^{B}(\mathbf{Y}_{22}^{A} + \mathbf{Y}_{22}^{B})\mathbf{Y}_{21}^{A}\mathbf{f}_1$$

$$\implies \quad \mathbf{f}_2^{eq} = (\mathbf{Y}_{22}^{A})^{-1}\mathbf{Y}_{21}^{A}\mathbf{f}_1 \tag{7.3}$$

Equation (7.3) shows that equivalent forces are indeed a property of substructure A.

The most practical method to determine the equivalent forces is by means of in-situ characterisation [5, 10]. The in-situ method makes use of indicator sensors on substructure B in order to determine the equivalent forces:

$$\mathbf{f}_2^{eq} = (\mathbf{Y}_{42}^{AB})^{-1}\mathbf{u}_4 \tag{7.4}$$

This method is easy to apply, as one only has to place sensors on structure B, determine $Y_{42}^{AB}$, and activate the source. Depending on the chosen amount of indicator sensors, the equivalent forces are solved either using a standard inverse or a pseudo-inverse. In other words, if the inverse problem is overdetermined (more $\mathbf{u}_4$ than $\mathbf{f}_2$) the equivalent forces are solved by minimising the sum of the squared error in $\mathbf{u}_4$:

$$\mathbf{f}_2^{eq} = (\mathbf{Y}_{42}^{AB})^{+}\mathbf{u}_4 \quad \implies \quad \mathbf{f}_2^{eq} = \arg\min ||\mathbf{u}_4 - \mathbf{Y}_{42}^{AB}\mathbf{f}_2|| \tag{7.5}$$

### 7.2.2 Equivalent vs. Blocked Force

In the theory above, the term equivalent forces is used. In literature, one often finds the denotation 'blocked' force, which refers to the blocking effect that these forces have on the active source when applied in opposite direction:

$$\mathbf{u}_4 = \mathbf{Y}_{41}^{AB}\mathbf{f}_1 - \mathbf{Y}_{42}^{AB}\mathbf{f}_2^{eq} = \mathbf{0}$$

In other words, $\mathbf{f}_2^{eq}$ represent the reaction forces if the source structure A were connected to a rigid boundary [3, 11, 12]. This indeed explains why the word "blocked" is commonly used, however it still leaves some room for interpretation. As stated before, the number of indicator DoFs is typically larger than the number of DoFs of the interface. This number is in turn bounded by a maximum of 6 per coupling point (3 translations and 3 rotations), assuming that the structures are rather stiff in the area where they interconnect. It is known that different set of forces can be found that represent the vibrations of the source that also function as 'equivalent' forces (see for instance [13]). In this study we use 6-DoF virtual point forces, which ensures that all translational forces as well as rotational moments are available for the characterisation. This way, if the equivalent forces are defined on the basis of these 6-DoF-per-point sets, it is fair to say that these forces are indeed blocking the interface in all possible directions. Therefore, we will continue with referring to $\mathbf{f}_2^{eq}$ by blocked forces.

## 7.3 Source Characterisation

Although Eq. (7.5) gives the impression that determining blocked forces is a straight-forward job, many difficulties arise when trying to correctly solve the inverse problem when using experimental data. Many of the problems concerning the calculation of blocked forces comes down to the effect of measurement noise and the inversion of $\mathbf{Y}_{42}^{AB}$, as will be explained further in the coming section.

### 7.3.1 Numerical vs. Experimental Characterisation

In the simplified world of numerical models no noise will be present, and thus solving for the blocked forces will be easy and correct. Linear algebra tells us that the only requirement for solving Eq. (7.5) is that the matrix $\mathbf{Y}_{42}^{AB}$ is full rank. In order to achieve a full-rank $\mathbf{Y}_{42}^{AB}$, the amount of indicator sensors $\mathbf{u}_4$ should be larger or equal to the number of forces that have to be identified and the columns of $\mathbf{Y}_{42}^{AB}$ should be linearly independent. Linear independent columns mean that each force of $\mathbf{f}_2^{eq}$ gives a linearly independent response at $\mathbf{u}_4$. When looking at a single frequency bin for which Eq. (7.5) is solved, this means that in order to get a full-rank matrix $\mathbf{Y}_{42}^{AB}$, 'enough' dynamics should be present. Theoretically, this means that the amount of eigenmodes of the system participating at this frequency bin should be higher than the amount of forces $\mathbf{f}_2^{eq}$ used for the characterisation. If the amount of modes participating at a frequency bin is too small, a linear dependence will exist between the columns of $\mathbf{Y}_{42}^{AB}$, as simply not enough dynamic information is available to create linearly independent responses.

For a numerical model this criterion should not pose a problem as each mode of the system will have some (albeit very small) contribution at each frequency bin. This means that having a numerical model with $n$ eigenmodes allows you to solve Eq. (7.5) for $n$ blocked forces, as long as the amount of sensors is equal or larger than $n$. As numerical models often consist of thousands of DoFs, more than enough dynamic information is available and solving for blocked forces is a straightforward process.

A real-life structure theoretically has an infinite amount of dynamics, but the presence of noise in the measurement results in much of the dynamics being unmeasurable. In order to show the effect that noise has on the resulting characterisation, a theoretical expansion of the measured data in a noise and signal part is analysed in the following section.

### 7.3.2 Blocked Force Noise

Let us consider the measurements and computational steps used to perform a source characterisation. Firstly an FRF measurement is required to determine the FRF matrix of transfer paths $\mathbf{Y}_{42}^{AB}$. Secondly an operational measurement is required in which the responses at the indicator DoFs $\mathbf{u}_4$ is measured for a certain load case of the source. Noise has an effect on both of these measurements, however the effect of noise on $\mathbf{Y}_{42}^{AB}$ is outside the scope of this paper.[1]

Let us consider a set of operational data $\mathbf{u}_4^{meas}$ that is corrupted with sensor noise. This means that the measured $\mathbf{u}_4^{meas}$ is a combination of both the true $\mathbf{u}_4^{signal}$ belonging to the blocked forces $\mathbf{f}_2^{eq}$ and the sensor noise $\mathbf{u}_4^{noise}$.

$$\mathbf{u}_4^{meas} = \mathbf{u}_4^{signal} + \mathbf{u}_4^{noise} \tag{7.6}$$

Using these measured responses $\mathbf{u}_4^{meas}$, the blocked forces $\mathbf{f}_2^{meas}$ are calculated:

$$\mathbf{f}_2^{meas} = (\mathbf{Y}_{42}^{AB})^+ \mathbf{u}_4^{meas} = (\mathbf{Y}_{42}^{AB})^+ (\mathbf{u}_4^{signal} + \mathbf{u}_4^{noise}) \tag{7.7}$$

By assuming the physical world acts as a linear system, the following expansion can be made:

$$\mathbf{f}_2^{meas} = (\mathbf{Y}_{42}^{AB})^+ \mathbf{u}_4^{signal} + (\mathbf{Y}_{42}^{AB})^+ \mathbf{u}_4^{noise} \tag{7.8}$$

---

[1]The effect of noise on the measurement of $\mathbf{Y}_{42}^{AB}$ is probably of minor importance, due to the fact that higher responses at the sensors can be generated using an impact or shaker measurement. This renders the influence of noise on the FRF measurement negligible.

$$\mathbf{f}_2^{\text{meas}} = \mathbf{f}_2^{\text{eq}} + \mathbf{f}_2^{\text{noise}} \tag{7.9}$$

Equation (7.9) shows how the calculated blocked forces $\mathbf{f}_2^{\text{meas}}$ using a noisy measurement are simply built up from a part corresponding to the true blocked forces $\mathbf{f}_2^{\text{eq}}$ and a noise part $\mathbf{f}_2^{\text{noise}}$ which we shall refer to as *blocked force noise*. The blocked force noise corresponds to the blocked forces that are calculated using a noise measurement on the sensors $\mathbf{u}_4$, i.e. with the source deactivated. Using this noise measurement, the blocked force noise can be calculated by solving Eq. (7.3).

To achieve that the calculated blocked forces are equal to the true blocked forces ($\mathbf{f}_2^{\text{meas}} = \mathbf{f}_2^{\text{eq}}$), two possibilities with a different physical interpretation are considered:

1. Increase the blocked force $\mathbf{f}_2^{\text{eq}}$ with respect to the blocked force noise $\mathbf{f}_2^{\text{noise}}$
2. Reduce the blocked force noise $\mathbf{f}_2^{\text{noise}}$ with respect to the blocked force $\mathbf{f}_2^{\text{eq}}$

The first case describes a situation in which the blocked forces are much larger than the blocked force noise. A physical interpretation for this is that the source ($\mathbf{f}_1$) is exciting the structure in such a manner that high blocked forces are required, thus minimising the influence of the blocked force noise on the results. The excitation levels of the source are however not tunable, as it is simply a property of the load case. As maximising $\mathbf{f}_2^{\text{eq}}$ is not possible (and probably the thing you are trying to prevent when doing TPA measurements), an alternative is to instead minimise the blocked force noise, as is defined by case two. The minimisation of these blocked forces will be dealt with in the next section.

### 7.3.3 Minimising Blocked Force Noise

Minimising the blocked force noise comes down to minimising the solution of $(\mathbf{Y}_{42}^{\text{AB}})^+\mathbf{u}_4^{\text{noise}}$. The outcome of this inverse operation can be minimised by either minimising the amount of sensor noise $\mathbf{u}_4^{\text{noise}}$ or by wisely choosing your measurement setup that defines the FRF matrix $\mathbf{Y}_{42}^{\text{AB}}$. As the sensor noise relates to the total noise picked up by the sensor, cabling, DAQ system etcetera, proper sensor selection in combination with minimising electrostatic interference is the main influence an experimentalist has on this noise level. However, the experimentalist does have a certain influence on $\mathbf{Y}_{42}^{\text{AB}}$. The DoFs for the blocked forces are prescribed by the virtual point (i.e. the 3 forces and 3 moments centred in the coupling point), but depending on the selection of the amount of sensors and their location, $\mathbf{Y}_{42}^{\text{AB}}$ will have certain properties which will be discussed next.

#### 7.3.3.1 Matrix Conditioning and Singular Values

Looking in more detail at how $\mathbf{Y}_{42}^{\text{AB}}$ is built up, reveals which parameters mostly influence the magnitude of the blocked force noise. Two aspects that are often used to analyse the properties of a matrix, especially when dealing with inverse problems, are the condition number and the singular value decomposition (SVD).

The condition number shows the amount of linear dependence that exists between the columns of matrix $\mathbf{Y}_{42}^{\text{AB}}$. A high condition number indicates that there is a high linear dependence between the columns of $\mathbf{Y}_{42}^{\text{AB}}$. It can thus be understood as some of the blocked forces showing a similar response at the indicator sensors $\mathbf{u}_4$, making it difficult to observe the difference between an excitation by $f_{2,i}^{\text{eq}}$ and a second excitation $f_{2,j}^{\text{eq}}$. As a result, if one wants to identify these blocked forces using responses at $\mathbf{u}_4$, a small error in $\mathbf{u}_4$ may lead to a large amplification in the blocked forces, as will be explained next. A high condition number is a good indication that a problem exists, but it does not explain precisely what is happening.

To get a better understanding, one can use a singular value decomposition of $\mathbf{Y}_{42}^{\text{AB}}$. The singular value decomposition can be written as follows:

$$\mathbf{Y}_{42}^{\text{AB}} = \mathbf{U}\boldsymbol{\Sigma}\mathbf{V}^{\mathbf{T}} \tag{7.10}$$

with $\mathbf{U}$ being the matrix with left singular vectors, $\mathbf{V}$ the matrix with right singular vectors and $\boldsymbol{\Sigma}$ the matrix with the singular values on the diagonal. The pseudo-inverse of $\mathbf{Y}_{42}^{\text{AB}}$ can now be written as follows:

$$(\mathbf{Y}_{42}^{\text{AB}})^+ = \mathbf{V}\boldsymbol{\Sigma}^+\mathbf{U}^{\mathbf{T}} \tag{7.11}$$

Expressing $\mathbf{f}_2^{\text{noise}}$ using this SVD expansion gives:

$$\mathbf{f}_2^{\text{noise}} = (\mathbf{Y}_{42}^{\text{AB}})^+ \mathbf{u}_4^{\text{noise}} = \mathbf{V}\mathbf{\Sigma}^+ \mathbf{U}^T \mathbf{u}_4^{\text{noise}} \tag{7.12}$$

To see the effect that a single singular value has on the level of blocked force noise, $\mathbf{u}_4^{\text{noise}}$ is assumed to be equal for all sensors DoF's of $\mathbf{u}_4$. Using Eq. (7.12) it can be reasoned that the magnitude of a singular value $\sigma_i \triangleq \Sigma_{ii}$ determines how much of the noise measured on the space spanned by $\mathbf{U}_i$ is amplified to the forces that excite this displacement space. If $\sigma_i$ has a very low value, its inverse in Eq. (7.12) will be large, meaning that a high blocked force noise can be expected for the forces that excite the displacement space belonging to $\sigma_i$. The smallest singular value of $\mathbf{Y}_{42}$ belongs to the displacement space that is least measured by the indicator sensors, and for the largest the opposite is true. A low singular value can be expected when two elements from $\mathbf{f}_2^{\text{eq}}$ have a very similar response at $\mathbf{u}_4$ or when a force from $\mathbf{f}_2^{\text{eq}}$ has a very low contribution to the excitation of the structure, in both cases rendering the forces badly observable using $\mathbf{u}_4$.

As a result of this, a good indication of the magnitude of the blocked force noise are the magnitudes of the smallest singular values of $\mathbf{Y}_{42}^{\text{AB}}$. In general, a higher condition number indicates the presence of a low singular value, resulting in an increase of the total blocked force noise. Therefore, reducing the condition number also reduces the magnitude of the blocked force noise.

#### 7.3.3.2 Blocked Force Signal-to-Noise Ratio

In order to get an indication of the quality of the calculated blocked forces, use can be made of a blocked force noise ratio. Rewriting Eq. (7.9) into a ratio gives:

$$\left| \frac{f_{2,i}^{\text{eq}}}{f_{2,i}^{\text{noise}}} \right| = \left| \frac{f_{2,i}^{\text{meas}}}{f_{2,i}^{\text{noise}}} \right| - 1 \tag{7.13}$$

This calculation will show for each element $i$ of the blocked forces a ratio between the useful information and noise. This ratio can easily be calculated using the calculated blocked forces and the blocked forces obtained from a noise measurement. A fraction of 0 will mean that the calculated blocked forces are solely the blocked force noise, and a value of infinite will tell you that the calculated blocked forces are the true blocked forces. Everything in between shows the ratio of blocked force signal-to-noise present in calculating the blocked forces.

### 7.3.4 Practical Implementation

Concluding from the previous section there are two rudimentary choices that influence the linear dependence and are a direct choice of the experimentalist: the sensor location with respect to the blocked forces and the amount of sensors used. The influence of both of these will be discussed in the following section.

#### 7.3.4.1 Sensor Distance

An empirically determined rule of thumb is that placing sensors closer to the forces that one wants to identify increases the linear independence, and thus decreases the condition number of the matrix $\mathbf{Y}_{42}^{\text{AB}}$ that has to be inverted [14]. The linear dependence increases as the sensors are moved further away from the location where the forces are applied due to a "blurring" effect present in the FRF. Intuitively this make sense: If you want to measure a difference between two sources that are placed close together, gut feeling tells you to measure close to these sources. When you are measuring further away, both sources will be much more difficult to distinguish. Theoretically this effect of blurring can also be explained by the reduced amount of anti-resonances when one moves further away from the excitation point [15, 16].

The physical reason behind this reduction in anti-resonances can be understood by looking at the two extreme cases, namely the driving point FRF ($Y_{ii}$), and a transfer point FRF ($Y_{ji}$) far away from the excitation point. To calculate the admittance $Y_{ji}$, the participation of each mode is added to the total, and the modal sign of each added mode will influence the final result. An example of the admittance calculated from two modes of a 2-DoF mass-spring system without damping
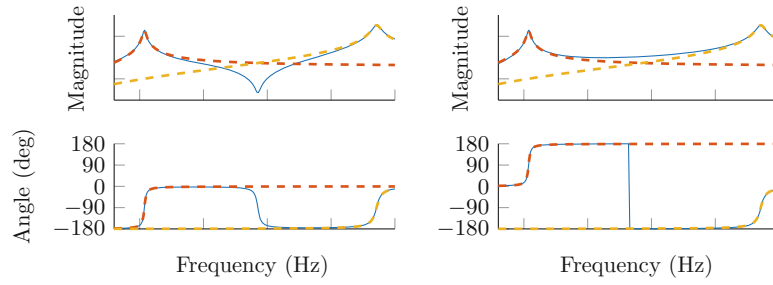
**Fig. 7.2** Accelerance plot of (**a**) Driving point FRF $Y_{ii}$, in which an antiresonance is visble at the point where both modal contributions (*dashed*) have the same magnitude (**b**) Transfer FRF $Y_{ji}$, in which an minimum is visible at the location where both modal contribution have the same magnitude

is shown in Eq. (7.14) and visualized by Fig. 7.2.

$$Y_{ii} = \frac{\mathbf{x}_{i,1}\mathbf{x}_{i,1}}{\omega_1^2 - \omega^2} + \frac{\mathbf{x}_{i,2}\mathbf{x}_{i,2}}{\omega_2^2 - \omega^2} \tag{7.14a}$$

$$Y_{ji} = \frac{\mathbf{x}_{j,1}\mathbf{x}_{i,1}}{\omega_1^2 - \omega^2} - \frac{\mathbf{x}_{j,2}\mathbf{x}_{i,2}}{\omega_2^2 - \omega^2} \tag{7.14b}$$

In these equations $\mathbf{x}_{i,n}$ is the eigenvector of mode $n$ at index $i$ and $\omega_n$ is the eigenfrequency of mode $n$. The modal sign of a mode is determined by the sign of the eigenmode at both the receiving and exciting DoF. When two consecutive modes have the same modal sign, an antiresonance will be present as can be seen in the left plot of Fig. 7.2. The yellow and red dotted lines represent the modal participation of mode 1 and 2, and at the point where they have the same magnitude they exactly cancel each other out, as can be reasoned using Eq. (7.14a). When the two modes have a different modal sign there will just be a minimum, and no antiresonance, as the two modal participations are simply added. The sign of the modes is determined by the value of the eigenvector at both the exciting and receiving node. This means that at a driving point there will always be an anti-resonance visible (Fig. 7.2a) as the square of the eigenvector value will always be positive. For a transfer FRF this is however not necessarily true. Depending on the location, modal contributions may be positive or negative, resulting in an FRF with sometimes an antiresonance and sometimes a minimum (Fig. 7.2b). Statistically it can be shown that when one moves the receiving and exciting point further apart, the chances of two consecutive modes differing in sign increases [16], resulting in what we observe as a 'blurred' FRF.

In practice this means that when the indicator sensors $\mathbf{u}_4$ are moved further away from the blocked forces, less difference can be observed between the different blocked forces. As a result, the indicator responses due to different components of $\mathbf{f}_2^{eq}$ will show a higher resemblance. Due to the higher resemblance, the value of the lowest singular value will decrease, increasing the conditioning of the matrix $\mathbf{Y}_{42}^{AB}$, in turn increasing the blocked force noise level.

### 7.3.4.2  Numerical Example

Using a numerical model of a beam consisting of 1600 nodes the effect that sensor distance has on the conditioning of the matrix $\mathbf{Y}_{42}^{AB}$ is visualised. The conditioning of $\mathbf{Y}_{42}^{AB}$ is evaluated for in total 6 different sensor groups, consisting of 12 DoF each. For this numerical example five forces have to be determined, placed on two nodes in the x, y and z-direction. The results of this numerical study are shown in Fig. 7.3. The left figure shows the condition number of $\mathbf{Y}_{42}^{AB}$ for the different sensor-sets. An increase in the condition number of a factor $1 \times 10^3$ can be observed for the position at the far end of the beam compared to the position close to the forces. The norm of the blocked force noise for the different sensor-sets is also calculated for a noise input of $1\,\mathrm{m\,s^{-1}}$, and plotted in the right figure of Fig. 7.3. The norm of the blocked force noise varies with a factor $1 \times 10^4$, with the sensors closest to the forces performing the best. This numerical example indeed confirms the theory that sensors closer tot the blocked forces show the least amount of blocked force noise.

An interesting observation is that this effect is only visible when a significant linear dependence exists between the columns of the matrix $\mathbf{Y}_{42}^{AB}$, i.e. when some of the components of $\mathbf{f}_2^{eq}$ show a similar response at $\mathbf{u}_4$. When the same numerical case is evaluated with a subset of the forces of $\mathbf{f}_2^{eq}$, no difference in conditioning and blocked force noise norm is found forthe
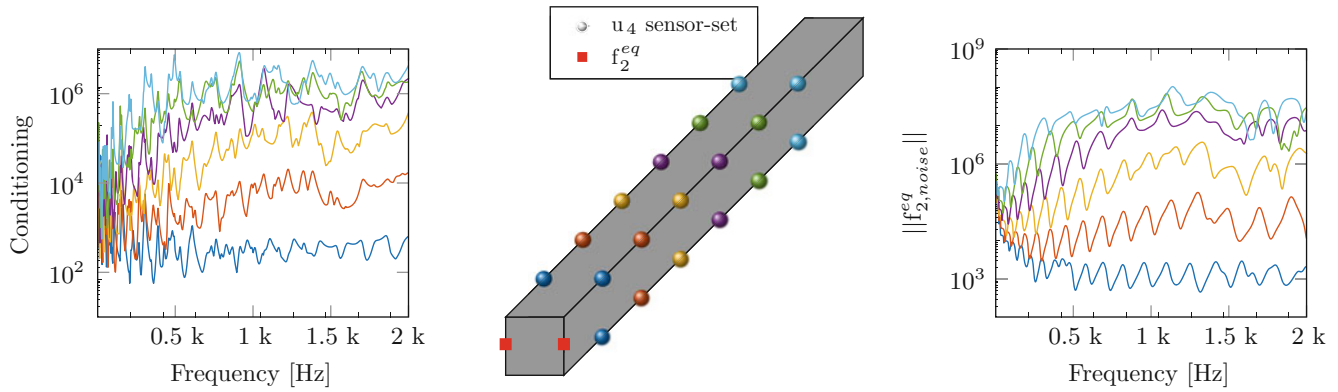
**Fig. 7.3** Conditioning of $\mathbf{Y}_{42}$ (*left*) and norm of the blocked force noise (*right*) for a numerical beam model for different sensor sets (colours are linked between graph and diagram)

different sensor distances. This logically makes sense, as forces that excite the structure in a similar manner will look more and more similar when moving further away from them, due to the blurring effect. Forces that show a distinctly different response will be much less influenced by the blurring effect.

### 7.3.4.3 Sensor Quantity

If an experimentalist is lucky enough to have plenty of sensors available for his/her measurement, it is a possibility to use a set of indicator sensors that is larger than the amount of forces that have to be identified, resulting in a overdetermined problem. The effect of overdetermination however depends on whether new dynamic information can be measured by the extra sensors, thus decreasing the condition number of the matrix $\mathbf{Y}_{42}^{\mathrm{AB}}$, and minimising the blocked force noise. One would expect to observe more and more information by the addition of each sensor, until a certain point at which all possible information is observed. This is further addressed in Sect. 7.4.

### 7.3.4.4 Matrix Regularisation

Matrix regularisation is an often used tool to improve the results of the inversion problem. Many types of regularisation methods exists, with the two most common being truncated singular value decomposition and Tikhonov regularisation [9]. All regularisation methods however come down to rejecting or minimising the solution belonging to the smallest singular value or a set of smallest singular values. In an optimal case, the error due to the discarding of the lowest singular value will be much smaller than the error due to the sensitivity to the other errors [17].

As discussed in the theory, the smallest singular value of $\mathbf{Y}_{42}$ belongs to the displacement space that is least measured by the indicator sensors. It can be reasoned that rejecting this displacement space from the solution, will result in a characterisation that is build up without the part of the blocked forces that is responsible for the excitation of this displacement mode. If one is purely interested in the blocked forces that are of the greatest influence on the assembly used for the characterisation, regularisation could help out to get a better conditioning of the inverse problem, but due to the fact that a certain set of blocked forces is being left out of the solution, it may render the blocked forces useless to be used as a unique set to describe the source for any other combination than AB.

## 7.4 Experimental Case Study

In the coming section the theory that has been discussed in the previous section will be applied to an experimental case study. A graphical render of the structure that was constructed for this specific task is visible in Fig. 7.4.
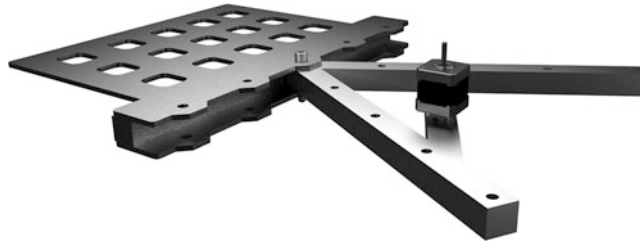
**Fig. 7.4** Artist impression of substructure A and B used for the experimental measurements, including the stepper motor that functions as the vibration source
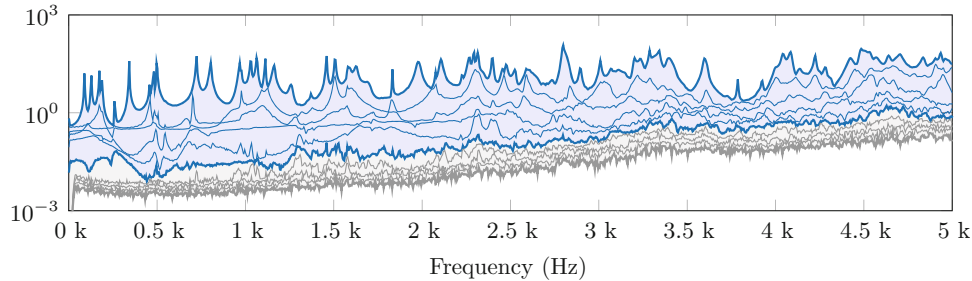


**Fig. 7.5** CMIF of $\mathbf{Y}_{42}^{\mathrm{AB}}$ for 15 indicator DoFs $\mathbf{u}_4$ as a result of 16 excitations $\mathbf{f}_2$ at the A-side

### 7.4.1 Measurement Setup

The structure used for the measurements consists of a substructure A, having the shape of an A-frame, and a structure B being a plate-like structure. Structure A and B can be coupled using one or two coupling points, by simply rotating the A-frame (the single point coupling is shown in the figure). A vibration source is used in the form of a NEMA 17 stepper motor, often used in the 3D printing industry. This stepper motor is controlled by an Arduino DUE with a Pololu A4988 stepper motor driver using the PWM protocol. A Müller-BBM PAK MKII was used for data acquisition in combination with 11 tri-axial PCB 356B21 sensors. The stepper motor PWM signal was connected to a tacho-pulse input channel of the DAQ system, allowing for easy speed monitoring and order tracking of the stepper motor. All measurements were done in a free-floating environment.

Two types of measurements have been performed on structure AB: (1) impact hammer measurements to determine the admittance FRFs $\mathbf{Y}_{42}^{\mathrm{AB}}$ from the virtual point to the receiving indicator sensors and (2) operational measurements with the stepper motor running for various load cases to determine $\mathbf{u}_4$. The operational measurements consisted of the stepper motor rotating at various constant speeds, doing a continuous sweep and lastly a discrete sweep, in which the motor speed is increased with 5% every 3 s. The discrete sweep is especially useful for source characterisation, as it provides many loadcases with a constant source excitation.

### 7.4.2 Bottleneck Effect

In order to show that indeed a virtual point can be used to describe the coupling between the substructures, the presence of the bottleneck effect is analysed using the complex mode indicator function (CMIF) [18] of the FRF matrix. The bottleneck effect is a consequence of the rigidity assumption of the interface, which is what the virtual point concept is based on [1]. It can be understood that a maximum of 6 different modes can be visible in the connecting substructure B, independent of the amount of modes being excited in substructure A, due to the fact that they are connected with a 6-DoF interface. If this bottleneck effect is indeed present, the choice for a virtual point with 6 DoFs for the blocked forces is made legitimate.

A CMIF is calculated for 24 response DoFs on substructure B to 16 excitations on substructure A. Figure 7.5 shows that up to approximately 1000 Hz the responses on substructure B are dominated by a maximum of 6 modes per frequency bin, clearly confirming the presence of the bottleneck effect. Onwards from 1000 Hz the amount of modes present at each
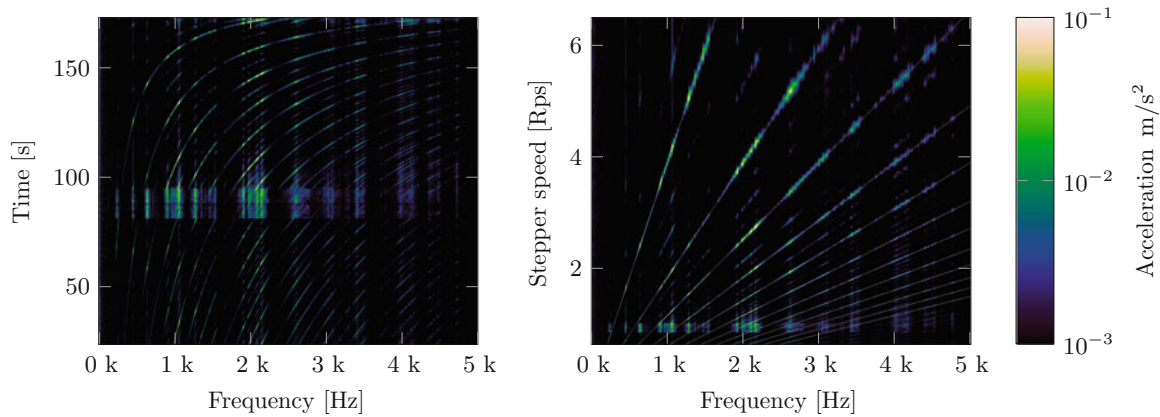
**Fig. 7.6** Waterfall diagram (*left*) and Campbell diagram (*right*) of $\mathbf{u}_3$ response in z-direction

frequency bin in the system increases as the interface starts to show more flexibility, and thus acts less as a bottleneck. Theses results thus show that a 6 DoF virtual point can be used for the blocked forces.

### 7.4.3 Typical BF-TPA Application

#### 7.4.3.1 Dominance of Motor Orders

A first look at the operational results show that the stepper motor excites the structure at specific orders, and is therefore not a broadband source. Using the continuous sweep of the stepper motor, a waterfall and Campbell diagram (including order tracking) can be constructed. A typical waterfall and Campbell diagram of a sensor on the B-side of the assembly AB is shown in Fig. 7.6.

Both diagrams show that the response of the sensor is almost completely built up using the orders of the stepper motor. As the stepper orders are dominant in the sensor responses, the same would be expected for the blocked forces.

#### 7.4.3.2 Blocked Force Characterisation

Using the FRF measurement of $\mathbf{Y}_{42}^{AB}$ and an operational measurement, a source characterisation for one of the many load cases of the stepper motor can be performed using the theory described. Using the measured $\mathbf{u}_4$ responses and the FRF matrix $\mathbf{Y}_{42}^{AB}$, Eq. 7.5 is solved, giving a set of blocked forces that characterise the loadcase. In addition, using a noise measurement in which the source is turned off, the blocked force noise can be determined by again solving Eq. (7.5) with $\mathbf{u}_4$ being $\mathbf{u}_4^{noise}$. A typical result of such a characterisation and blocked force noise calculation that were done using a set of 5 sensors to determine 6 blocked forces is shown in Fig. 7.7.

The top plot of Fig. 7.7 shows the results for a component of the calculated blocked forces ($\mathbf{f}_2^{meas}$), namely the blocked force acting in the z-direction of the virtual point (blue). In addition, also the blocked force noise that was calculated for this component is visualized in the same plot (red). The plot shows that indeed the characterisation can be interpreted as being a combination of the blocked force noise and a blocked force part, as was stated by Eq. (7.9). The bottom plot shows a waterfall diagram of the same blocked force component as was portrayed in the top plot. The waterfall diagram is build up of in total 32 loadcases over time. The waterfall diagram clearly visualizes how the blocked force noise dominates the characterisation at all of the characterisations and thus minimizing the effect of the blocked force noise would certainly be an advantage for the quality of a characterisation.

#### 7.4.3.3 Response Reconstruction

Using a characterisation such as the one that was shown in the previous chapter, one can reproduce the response at a reference DoF $\mathbf{u}_3$ using the transfer path $\mathbf{Y}_{32}^{AB}$. Performing this reconstruction and comparing it with the measured $\mathbf{u}_3$ will give an
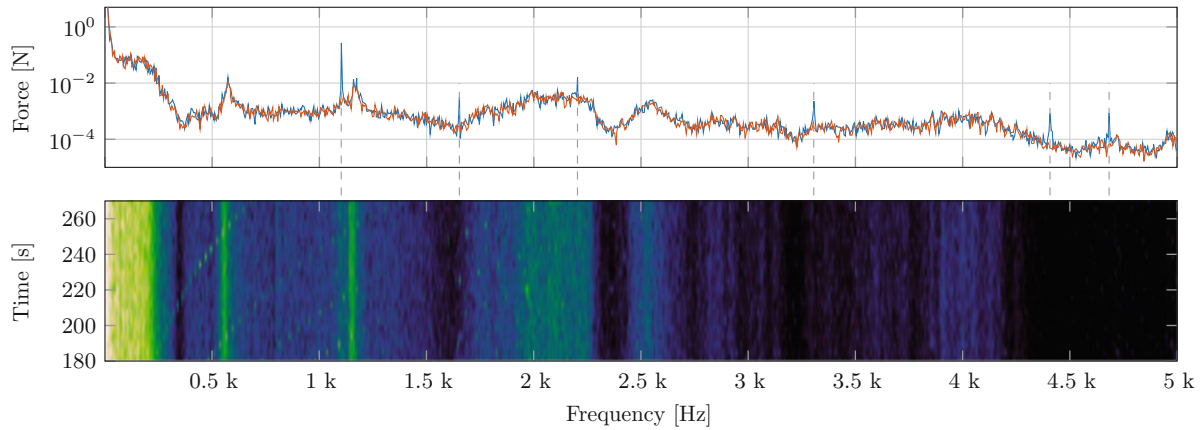
**Fig. 7.7** Typical characterisation result of a load case. *Top plot*: calculated $\mathbf{f}_2^{eq}$ component in z-direction for a load case (*blue*) and measured blocked force noise (*red*), including stepper orders (*dashed*), *bottom plot*: waterfall diagram of $\mathbf{f}_2^{eq}$ in z-direction for different loadcases with increasing stepper speeds over time
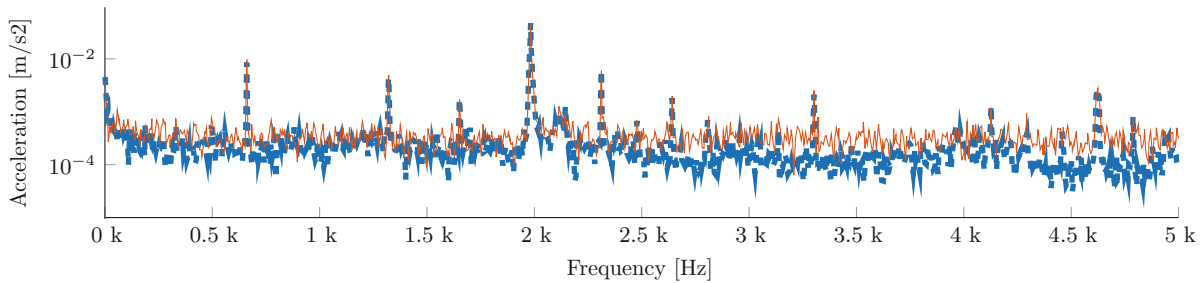


**Fig. 7.8** Typical reconstructed $\mathbf{u}_3$ (*blue*) and measured $\mathbf{u}_3$ (*red*)

indication if the characterisation is indeed capable of predicting the dynamic response at a location at structure B. Figure 7.8 shows a typical result for such a $\mathbf{u}_3$ reconstruction in combination with a measured $\mathbf{u}_3$.

The reconstructed and measured response are almost identical, which shows that the characterisation is capable of predicting the response at points in the structure that were not used to calculate the characterisation.

### 7.4.4 Sensor Placement

To study the effect that sensor placement has on the magnitude of the blocked force noise and thus overall quality of the characterisation, two configurations of the experimental structure are analysed. The first configuration that is analysed is the single point coupling as can be seen in the left image of Fig. 7.9. Secondly also a two-coupling configuration is analysed which is shown in the right image of Fig. 7.9.

#### 7.4.4.1 Single-Point Coupling

To evaluate the influence of the distance of the sensors on the quality of the characterisation using the single-point coupling configuration, five sensor-sets are evaluated at different locations on the structure B. Each sensor-set consists of five tri-axial sensors, which should result in a thoroughly overdetermined matrix $\mathbf{Y}_{42}^{AB}$ (15 × 6). The different sensor-set locations are shown in the left image of 7.9.

In order to compare the different sensor-sets, a noise and impact measurement are performed for each sensor-set, allowing one to calculate the blocked force noise in a similar manner as was done in the previous section. In order to compare the calculated blocked force noise of the different sensor-sets, use is made of the norm of blocked force noise, as this will give a clear indication of the total magnitude of the noise level. As the source is characterised using forces and moments, they will be compared separately.
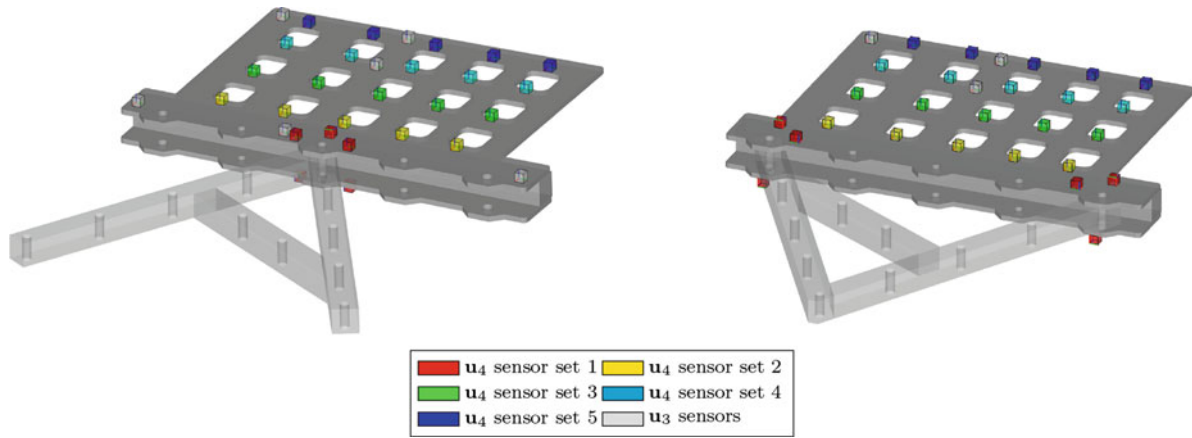
**Fig. 7.9** Sensor location groups. *Left*: single-point coupling configuration; *right*: two-point coupling configuration
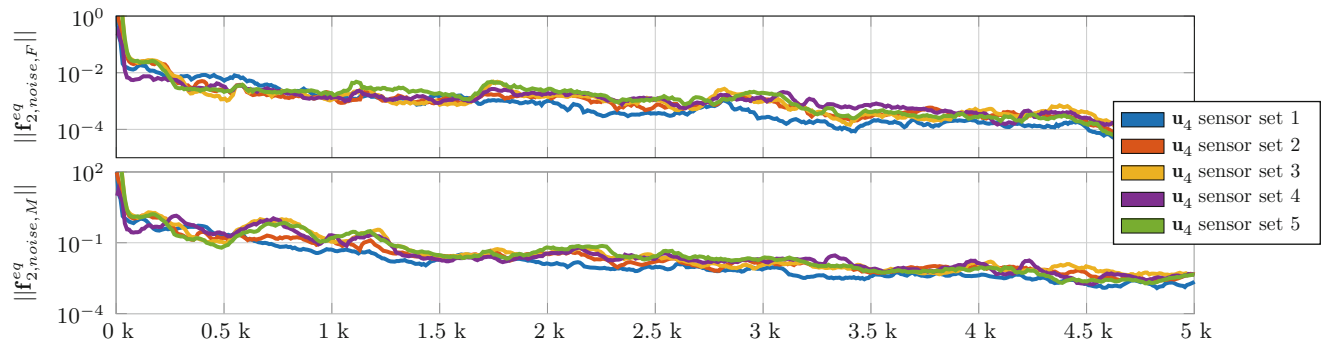


**Fig. 7.10** Comparison of blocked force noise norm (*top*) and moment norm (*bottom*) for different sensor distances in the single-point coupling configuration

Figure 7.10 shows a comparison of the norm of the blocked force noise, done separately for the forces and moments. Sensor-set 1 corresponds to the sensors placed closest to the blocked forces and sensor-set 5 to the set placed furthest away. Due to the fact that no clear difference is observed between the different sensor locations it can not be concluded whether placing sensor closer to the blocked forces is of any advantage, and that indeed the blurring effect described in Sect. 7.3 is applicable to experimental data. A minor improvement of the blocked force noise moments can be seen for sensors placed close to the blocked forces, but for the forces shown in the top figure the opposite can be concluded. A possible reason for the absence of any difference between the sensor location can be found in the results of the numerical beam analysis. The numerical analysis already showed that characterisation problems that have easily distinguishable blocked forces are almost not affected by sensor distance, as even at a large distance the forces are still distinguishable. As use is made of a virtual point for the blocked forces, the matrix $\mathbf{Y}_{42}$ shows a high amount of linear independence, as the six forces and moments excite the structure in linear independent manners. In order to show that indeed placing sensors close to the blocked forces is of an advantage, the characterisation has to be made more interesting by making use of a two-point coupling of structure AB as was shown in the right image of Fig. 7.9.

### 7.4.4.2 Two-Point Coupling

In order to analyse the two-point coupling, a similar measurement and calculation procedure was followed as for the single-point coupling. Again the norm of all the blocked force noise forces and moments is used as an indication of the quality of the characterisation.

Figure 7.11 shows the results for this analysis. Both the results for the forces and moments show that sensor set 1, which is placed closest to the virtual points, has a blocked force noise norm which is a factor 10 smaller than the other sensor sets. This means that indeed the sensor set placed closest to the blocked forces has the lowest amount of blocked force noise acting on the results, as was predicted in Sect. 7.3. Even more, all of the sensor-sets except set 1 generate a blocked force noise
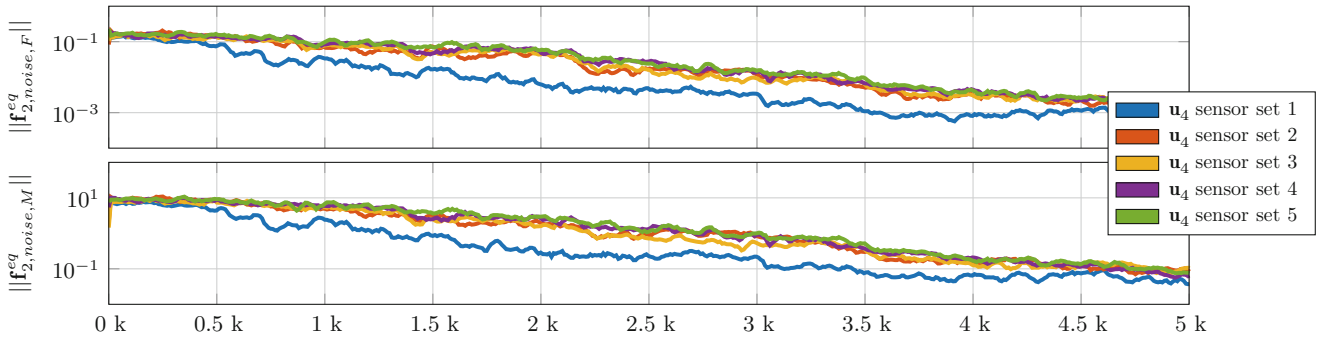
**Fig. 7.11** Comparison of blocked force noise (*top*) and moment (*bottom*) norm for different sensor distances in the two-point coupling configuration
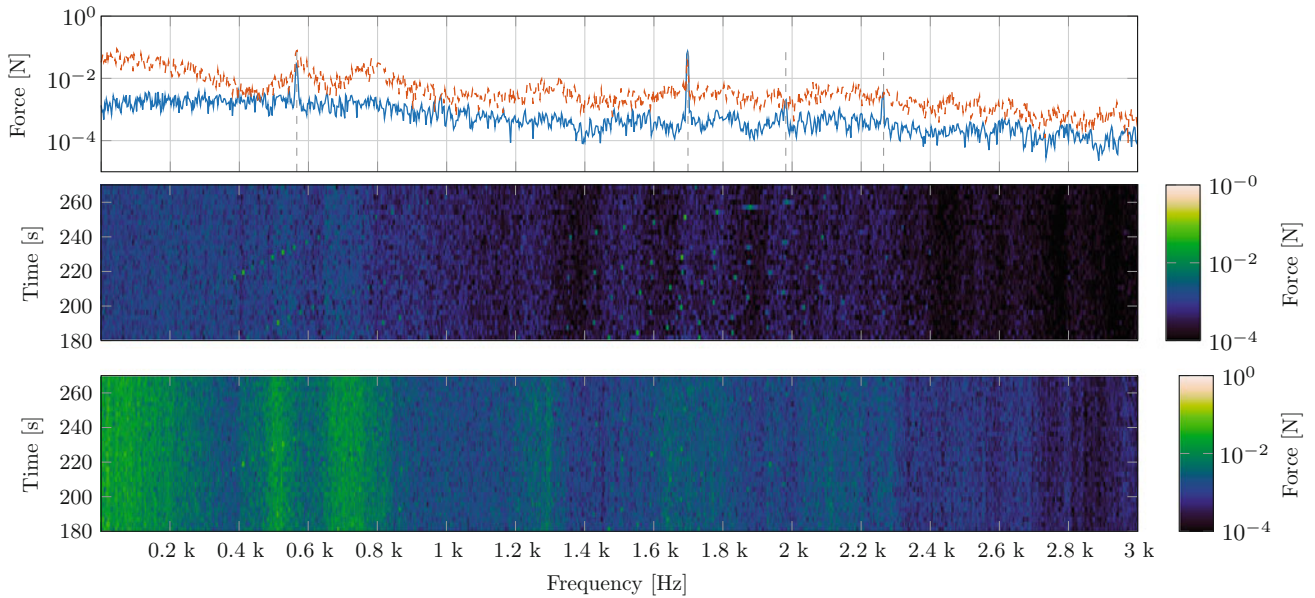


**Fig. 7.12** Comparison of characterisation $\mathbf{f}_2^{eq}$ in z-direction. Waterfall diagram of sensor set 1 is shown in the *middle plot*, and for sensor set 5 in the *bottom plot*. A *zoomed* in loadcase is presented in the *top plot*, showing the result for sensor-set 1 (*red*) and sensor-set 5 (*red*)

level that is in the same order of magnitude as the blocked force itself, rendering the characterisation useless. An example of this is shown in Fig. 7.12, which shows the blocked forces of the right coupling point in the z-direction determined with sensor-set 1 and 5. In the waterfall diagram shown in the middle plot (sensor-set 1), clear peaks are visible for each of the loadcases, corresponding to the orders of the stepper. The waterfall diagram of the bottom plot corresponds to the same blocked force component, but this time the characterisation is done using sensor-set 5. This waterfall diagram shows that the order peaks that were clearly visible using sensor-set 1 are now masked by the blocked force noise. A zoomed-in load case from the waterfall diagrams is shown in the top plot, and shows the characterisation for the same specific loadcase done by both sensor-set 1 and sensor-set 5. This plot clearly visualizes that the blocked force noise of sensor-set 5 is higher than the blocked forces that represent the characterisation of the source.

### 7.4.5 Sensor Overdetermination

#### 7.4.5.1 Blocked Forces

In order to study the effect of overdetermination of $\mathbf{Y}_{42}^{AB}$, the characterisation with sensor-set 1 is done with five, four, three and two sensors per virtual point for the single-point coupling. To eliminate the effect of the chosen sensor combinations, an average is taken of the $\binom{n}{5}$ possibilities that exist.

Figure 7.13 shows the norm of the blocked force/moment noise for different sensor amounts, normalised to the results for a set with two sensors. The first observation is that indeed, increasing the amount of sensors increases the quality of the result. The largest difference for the level of the blocked force noise is seen for the addition of one extra sensor, and every other additional sensor does improve the result, but not as significant as the first sensor. The question however remains if the sensor combinations are also able to correctly characterise a source when the number of sensors decrease, which is analysed in the next section.

#### 7.4.5.2 Response Reconstruction

A comparison of the reconstructed $\mathbf{u}_3$ using different amounts of sensor numbers is shown in Fig. 7.14. Firstly it can be observed that indeed the peaks are of equal magnitude of all the reconstructed $\mathbf{u}_3$ responses, meaning that indeed the stepper orders are equally reconstructed by each amount of sensors. The second observation is that a lot more noise is present in the reconstruction using the minimal amount of two sensors, which is what the results of Fig. 7.13 already showed us. Comparing the magnitude of the source characterisation with the noise level shows that a valid characterisation is not possible using just two sensors.
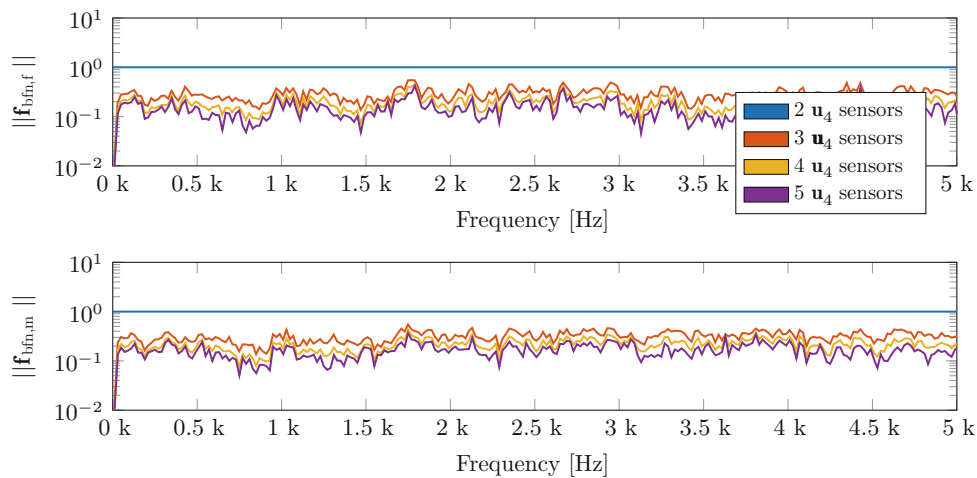


**Fig. 7.13** Effect of overdetermination on the norm of the blocked force noise for the forces (*top*) and moments (*bottom*), normalized to the results using two sensors
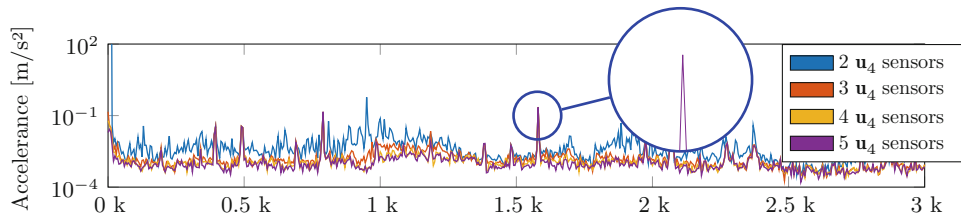


**Fig. 7.14** Typical reconstructed $\mathbf{u}_3$ result with different number of sensors used

## 7.5 Conclusion

This paper introduces a structured approach for the use of indicator sensors for the characterisation of a dynamic source using in-situ blocked force TPA. Using a combination of both theory, numerical testing,experimental measurements and the introduction of the blocked force noise, results have been found that show that sensor placement and sensor quantity have a large influence on the quality of the characterisation.

To minimise the blocked force noise and maximise the quality of the characterisation, the indicator sensors must be placed close to the forces that one wants to identify, and at least one additional sensor must be used for the overdetermination of the inverse problem. Although this paper mainly focusses on in-situ blocked force TPA, the insights obtained can also be applied to the matrix inverse method or any other type of force identification methods, in which the same type of inverse problem is solved.

## 7.6 Outlook

As for now, a structured approach is proposed which helps an experimentalist in deciding where to place the indicator sensors. Many future possibilities however exist, which can further improve the source characterisation procedure. Quantifying the quality of a characterisation using a ratio such as the blocked forces signal to noise ratio that was proposed in the theory section, would make for a good first step.

## References

1. van der Seijs, M.V., de Klerk, D., Rixen, D.J.: General framework for transfer path analysis: history, theory and classification of techniques. Mech. Syst. Signal Process. **68–69**, 217–244 (2016)
2. de Klerk, D., Rixen, D.J.: Component transfer path analysis method with compensation for test bench dynamics. Mech. Syst. Signal Process. **24**(6), 1693–1710 (2010)
3. van der Seijs, M.V., Pasma, E.A., de Klerk, D., Rixen, D.J.: A robust transfer path analysis method for steering gear vibrations on a test bench. In: Proceedings of the International Conference on Noise and Vibration Engineering (ISMA), Leuven (2014)
4. van der Seijs, M.V., Pasma, E.A., de Klerk, D., Rixen, D.J.: A comparison of two component TPA approaches for steering gear noise prediction. In: Dynamics of Coupled Structures. Proceedings of the 33rd IMAC, A Conference and Exposition on Structural Dynamics, vol. 4, chapter 7, pp. 71–79. Springer, New York (2015)
5. Moorhouse, A.T., Elliott, A.S., Evans, T.A.: In situ measurement of the blocked force of structure-borne sound sources. J. Sound Vib. **325**(4–5), 679–685 (2009)
6. de Klerk, D., Rixen, D.J., Voormeeren, S.N.: General framework for dynamic substructuring: history, review and classifcation of techniques. AIAA J. **46**(8), 1169–1181 (2008)
7. van der Seijs, M.V., van den Bosch, D.D., Rixen, D.J., de Klerk, D.: An improved methodology for the virtual point transformation of measured frequency response functions in dynamic substructuring. In: Papadrakakis, M., Papadopoulos, V., Plevris, V. (eds.) 4th ECCOMAS Thematic Conference on Computational Methods in Structural Dynamics and Earthquake Engineering (COMPDYN), Kos Island, pp. 4334–4347 (2013)
8. Thite, A.N., Thompson, D.J.: Selection of response measurement locations to improve inverse force determination. Appl. Acoust. **67**(8), 797–818 (2006)
9. Wang, J., Law, S.S., Yang, Q.S.: Sensor placement methods for an improved force identification in state space. Mech. Syst. Signal Process. **41**(1–2), 254–267 (2013)
10. Elliott, A.S.: Characterisation of structure borne sound source in-situ. Ph.D thesis, University of Salford (2009)
11. de Klerk, D.: Dynamic response characterization of complex systems through operational identification and dynamic substructuring. Ph.D thesis, Delft University of Technology (2009)
12. Rixen, D.J., Boogaard, A., van der Seijs, M.V., van Schothorst, G., van der Poel, T.: Vibration source description in substructuring: a theoretical depiction. Mech. Syst. Signal Process. **60–61**, 498–511 (2015)
13. Janssens, M.H.A., Verheij, J.W., Thompson, D.J.: The use of an equivalent forces method for the experimental quantification of structural sound transmission in ships. J. Sound Vib. **226**(2), 305–328 (1999)
14. Nelson, P.A., Yoon, S.-H.: Estimation of acoustic source strength by inverse methods: part I, conditioning of the inverse problem. J. Sound Vib. **233**(4), 639–664 (2000)
15. Wahl, F., Schmidt, G., Forrai, L.: On the significane of antiresonance frequencies in experimental structural analysis. J. Sound Vib. **219**(3), 379–394 (1999)
16. Ewins, D.J.: Modal Testing 2/E, 562 Seiten. John Wiley & Sons Inc (2009). ISBN:0863802184. http://www.ebook.de/de/product/18564154/d_j_ewins_modal_testing_2_e.html
17. Blau, M.: Inverse force synthesis: state of the art and future research. In: Proceedings of Inter-Noise (2000)
18. Allemang, R.J.: The modal assurance criterion (MAC): twenty years of use and abuse. In: Proceedings of the International Modal Analysis Conference (IMAC), Los Angeles, vol. 20, pp. 397–405 (2002)